Liu, W., Jin, M., Chen, C., and Chen, Q. 2015. "Optimization of air supply location, size, and parameters in enclosed environments through using a CFD-based adjoint method," Accepted by *Journal of Building Performance Simulation*,

Optimization of air supply location, size, and parameters in enclosed environments through using a CFD-based adjoint method

Wei Liu[a,b], Mingang Jin[b], Chun Chen[b], Qingyan Chen[b,a*]
[a]Tianjin Key Lab of Indoor Air Environmental Quality Control, School of Environmental Science and Engineering, Tianjin University, Tianjin 300072, China
[b]School of Mechanical Engineering, Purdue University, West Lafayette, IN 47905, USA
*Corresponding email: yanchen@purdue.edu

Optimal design of an indoor environment based on specific design objectives requires a determination of thermo-fluid control methods. The control methods include the air supply location, size, and parameters. This study used a CFD-based adjoint method to identify the optimal air supply location, size, and parameters. Through defining the air distribution in a certain area (design domain) as a design objective in a two-dimensional, ventilated cavity, the adjoint method can identify the air supply location, size, and parameters. However, the air supply location, size, and parameters were not unique, which implied multiple solutions. By using any of the air supply location, size and parameters identified as boundary conditions for forward CFD simulations, the computed air distribution in the design domain was the same as that used as a design objective. Thus, the computing costs did not depend on the number of design variables.

Keywords: shape optimization, adjoint method, inverse design

1. Introduction

A thermally comfortable and healthy indoor environment is typically achieved by conditioning buildings with heating, ventilating, and air-conditioning (HVAC) systems. Energy use by the HVAC systems accounts for over 40% of the total energy used in buildings in the United States, according to the 2011 Building Energy Data Book published by the U.S. Department of Energy. The energy accounted for 16% (16 quadrillion BTU/year) of the primary energy consumption in the United States in 2010. But even with such high energy consumption and carbon dioxide emissions, the indoor environment is actually very poor. Survey data from the International Facility Management Association (IFMA, 2003) shows that the predominant complaints from office occupants were "It's too hot and too cold, simultaneously." However, not only is the thermal environment poor, but studies have also found that 20% of the buildings have sick building syndrome (SBS) (Mendell, 1993; Menzies et al., 1994; Hedge et al., 1996). All these facts leave an element of doubt as to whether the current design of the indoor environment is appropriate. Besides, the traditional design method uses a "trial-and-error" process that is time consuming and the design could not be optimal. These issues should lead researchers and designers to optimize the indoor environment.

Recently, computational fluid dynamics (CFD), combined with optimization algorithms, has appeared for optimizing the design of an enclosed environment. These methods mainly include the CFD-based GA (genetic algorithm) (Zhou and Haghighat, 2009a, 2009b; Xue et al., 2013), the POD (proper orthogonal decomposition) method (Li et al., 2012, 2013), and the CFD-based adjoint method (Liu and Chen, 2014). The GA is superior for finding global optimal conditions (Holland, 1975). Some recent studies combined GA and energy simulation models to minimize building energy consumption that can be efficient (Kämpf et al., 2010; Nguyen and Reiter, 2014; Wright et al., 2014). But the combination of CFD and GA still requires too many CFD simulations. Thus, a typical optimal

design of an indoor environment would take a week or more to complete, which is too long to be accepted by a designer. In order to reduce the CFD simulation effort, POD, which uses 10 or fewer CFD simulations to describe the characteristics of indoor air distribution, is applied. In the offline stage, POD uses CFD simulations to obtain detailed information on the air distribution. Then, snapshots are sampled for constructing reduced-order air distributions. In the online stage, the reduced-order model is embedded in the optimization system, which can dramatically alleviate the computation effort (Rozza et al., 2007; Haasdonk and Ohlberger, 2011). The POD is fast; however, the method itself may not be accurate due to the nonlinear nature of an indoor environment.

The adjoint method computes the derivative of the design objective over the design variables to determine the search direction for optimization so that it only finds the local optimal solutions. The adjoint method requires less computing load than the CFD-based GA method. Besides, a CFD-based adjoint method can be more accurate than the POD technique as it directly solves the Navier-Stokes (NS) equations with a suitable turbulence model by using actual thermo-fluid boundary conditions. Liu and Chen (2014) have validated this method for finding optimal thermo-fluid boundary conditions in a two dimensional cavity. The results showed the capacity and high accuracy of this method, but the number of design variables in our previous study was limited.

With more design variables, the CFD-based adjoint method can achieve a better design for an indoor environment. The current design method for an indoor environment (ASHRAE, 2010) does not provide specific instructions for determining the exact location of the air supply diffuser or its size, which are very critical to know in determining air distributions. The design variables in the CFD-based adjoint method could include air supply location and size. This paper describes our effort in using the CFD-based adjoint method to determine air supply location, size, and parameters through implementing the method in OpenFOAM (open field operation and manipulation) (2007).

2. Method

In an enclosed environment, the air supply location, size, and parameters are critical in determining the air distributions. Thus, our effort is to identify the proper air supply location, size, and parameters for designing an indoor environment. This investigation used the CFD-based adjoint method for identifying the optimal air supply location, size, and parameters. The corresponding numerical algorithm used is also discussed.

2.1 CFD-based adjoint method

The CFD-based adjoint method uses the following processes to identify the optimal design variable ξ , which represents air supply location (x_{in}, y_{in}), size (h_{in}), and parameters (V_{in}, T_{in}) in this study. It forms a vector or a 1×5 matrix $\xi = (x_{in}, y_{in}, h_{in}, V_{in}, T_{in})$ and any mathematical operations involving ξ are matrix operations.

Step 1:

Establish the design objective in the occupied zone of a room and construct the corresponding objective function $O(p, V, T)$, which will be minimal with an optimal ξ. Objective function is actually a mathematical explanation for the design objective. One can construct various objective functions for a design objective. For example, the design objective can be the thermal comfort or air quality in the occupied zone of a room. The objective function can be constructed to make PMV or the age of the air very small with appropriate p, V, and T distributions in the occupied zone. For more examples of design objectives and objective functions, refer to the study by Zhou and Haghighat (2009).

Step 2:

The parameters in the objective functions (p, V, T) are calculated in our case by solving the NS equations, which are denoted by vector $S = (S_1, S_2, S_3, S_4, S_5) = (0, 0, 0, 0, 0)$:

$$S_1 = -\nabla \cdot V \tag{1}$$

$$(S_2, S_3, S_4)^T = (V \cdot \nabla)V + \nabla p - \nabla \cdot (2\nu D(V)) - \gamma \vec{g}(T - T_{op}) \tag{2}$$

$$S_5 = \nabla \cdot (VT) - \nabla \cdot (\kappa \nabla T) \tag{3}$$

Step 3:
With an initialized ξ, the initial $O(p, V, T)$ calculated in step 2 is often not minimal. The CFD-based adjoint method determines the derivative of the objective function over the design variables ($dO/d\xi$) in order to search for the trend in varying ξ that can lead to a smaller O. Since O is a function of the V, T, and p but not ξ, the gradient $dO/d\xi$ cannot be directly computed. Since ξ determines V, T, and p and further O, the adjoint method introduces a Lagrangian multiplier (p_a, V_a, T_a), which stands for adjoint velocity, temperature, and pressure, respectively, to make $dO/d\xi$ computable. The adjoint variables could be regarded as purely mathematical terms, but they do have physical significance. According to Giles and Pierce (2000), one way of looking at them is that they give the influence of an arbitrary source term on the functional of interest (the NS equations here). Then, this method uses an augmented objective function as:

$$L = O + \int_{\Omega} (p_a, V_a, T_a) S d\Omega \tag{4}$$

Since S = (0, 0, 0, 0, 0) in step 2, L actually equals O in Eq. (4). Therefore, finding ξ for minimizing O becomes finding ξ for minimizing the augmented objective function L. Our effort is to calculate the gradient $dL/d\xi$ instead of $dO/d\xi$. Considering the variation of ξ, the variation of L can be expressed as:

$$dL = \frac{\partial L}{\partial \xi} d\xi + \frac{\partial L}{\partial p} dp + \frac{\partial L}{\partial V} dV + \frac{\partial L}{\partial T} dT \tag{5}$$

To determine the gradient $dL/d\xi$, the adjoint variables (p_a, V_a, T_a) are chosen to satisfy:

$$\frac{\partial L}{\partial p} dp + \frac{\partial L}{\partial V} dV + \frac{\partial L}{\partial T} dT = 0 \tag{6}$$

Eq. (6) would eliminate the contribution of dp, dV, and dT in Eq. (5), then $dL/d\xi = \partial L/\partial \xi$ that is straightforward. Eq. (6) has to be fulfilled for any (dp, dV, dT) that is entailed by $d\xi$, which can be accomplished by setting the three partial derivatives on the left hand side at zero, respectively, which constructs three independent equations:

$$\frac{\partial L}{\partial p} = \frac{\partial O}{\partial p} + \int_{\Omega} (p_a, V_a, T_a) \frac{\partial S}{\partial p} d\Omega = 0 \tag{7}$$

$$\frac{\partial L}{\partial V} = \frac{\partial O}{\partial V} + \int_{\Omega} (p_a, V_a, T_a) \frac{\partial S}{\partial V} d\Omega = 0 \tag{8}$$

$$\frac{\partial L}{\partial T} = \frac{\partial O}{\partial T} + \int_{\Omega} (p_a, V_a, T_a) \frac{\partial S}{\partial T} d\Omega = 0 \tag{9}$$

After a number of integral transformation steps in these three equations, we have:

$$-\nabla \cdot V_a = 0 \tag{10}$$

$$-\nabla V_a \cdot V - (V \cdot \nabla)V_a - \nabla \cdot (2\nu D(V_a)) + \nabla p_a - T\nabla T_a + \partial O / \partial V = 0 \quad (11)$$

$$-V \cdot \nabla T_a - \nabla \cdot (\kappa \nabla T_a) + \partial O / \partial T = 0 \quad (12)$$

Eqs. (10), (11), and (12) are the final form of Eqs (7), (8), and (9), respectively. The reader can refer to Othmer (2008) for the detailed derivation procedure. Eqs. (10), (11), and (12) have unknown adjoint variables (p_a, V_a, T_a) and are called adjoint equations. Further, since Eq. (10) has the same form as the continuity equation in the NS equations, it is called adjoint continuity equation. Likewise, Eqs. (11) and (12) are called adjoint momentum equation and adjoint energy equation, respectively. Previous studies by Jameson (1995) and Jameson et al. (1998) have proven the solvability of the adjoint equations. The solutions for the adjoint equations will then be used to compute $dL/d\xi$, which can be expressed as:

$$\frac{dL}{d\xi} = \frac{\partial L}{\partial \xi} = \frac{\partial O}{\partial \xi} + \int_{\Omega} (p_a, V_a, T_a) \frac{\partial S}{\partial \xi} d\Omega \quad (13)$$

Since the NS equations $S = 0$ are solved numerically, S becomes the residuals of the corresponding solution to the NS equation. Then $\partial S/\partial \xi$ actually computes the partial derivative of the solution residuals of the NS equations with respect to the design variable ξ.

Step 4:

By using the simple steepest descent algorithm (Bryson and Ho, 1975), ξ can be updated by:

$$\xi_{new} = \xi_{old} + d\xi = \xi_{old} - \lambda [\frac{\partial O}{\partial \xi} + \int_{\Omega} (p_a, V_a, T_a) \frac{\partial S}{\partial \xi} d\Omega]^T \quad (14)$$

where λ is a positive constant. Then, the variation of L is always negative and the value of the objective function would always decrease. To compute $d\xi$ in Eq. (14), the adjoint equations (Eq. (10), (11), and (12)) are solved to determine the adjoint variables (p_a, V_a, T_a). Then, as the objective function O in this study is only a function of the *p, V, and T*, $\partial O/\partial \xi = 0$. Finally, one needs to evaluate the partial derivative $\partial S/\partial \xi$ in Eq. (14) in order to obtain $d\xi$.

2.2 Optimal design of the air supply location and size

The evaluation of the partial derivative $\partial S/\partial \xi$ in Eq. (14) requires differentiation of the algorithms that perform the computation of S (Sokolowski and Zolesio, 1992; Jimack, 1997). When ξ denotes air supply parameters, the partial derivatives can be evaluated by discretizing the S with the finite volume method (FVM) (Liu and Chen, 2014). In this paper, ξ denotes the air supply location and size as well. Mathematically, this study sets ξ as the coordinates of the nodes located on the boundary of the air supply diffusers. The discretization of S by FVM would lose the information of the coordinates of the mesh nodes and could not be applied to computing $\partial S/\partial \xi$.

Our literature review found three common methods that could be used to evaluate $\partial S/\partial \xi$ when ξ represents node coordinates: the chain rule of differentiation (Wikipedia), the finite difference method (FDM), and the finite element method (FEM). The chain rule of differentiation is mainly implemented in automatic differentiation software (Griwank, 2000). It allows functions such as S to be differentiated with respect to the input parameters such as ξ to evaluate the derivative $\partial S/\partial \xi$ as the output. This technique is powerful and derivatives of an arbitrary order can be computed automatically. Unfortunately, the automatic differentiation software is not generally efficient and mature tools of this kind are not available (Schneider, 2006). The FDM and FEM are mainly implemented by hand coding. The FDM (Gill et al., 1981; Gunzburger, 2003) requires minimal work

to program, but it is inefficient as the time in evaluating this derivative is proportional to the number of design variables. Later, Schneider and Jimack (Schneider and Jimack, 2008) simply discretized the NS equations by FEM to compute $\partial S/\partial \xi$. The discretization produces two non-constant parts with respect to the node positions that make the derivative $\partial S/\partial \xi$, which can be computed directly. Therefore, this study discretized the NS equations by FEM to evaluate $\partial S/\partial \xi$.

In applying the FEM to discretize S, this study chose the shape functions, N, as the basis functions. Considering the energy equation in the NS equations as an example, the discrete equation by FEM for node j can be expressed as:

$$S_{5,j} = \int_{\Omega} \kappa \nabla T \cdot \nabla N_j d\Omega + \int_{\Omega} (V \cdot \nabla T) N_j d\Omega \tag{15}$$

For the diffusion term in Eq. (15), we have:

$$\begin{aligned} \int_{\Omega} \kappa \nabla T \cdot \nabla N_j d\Omega &= \kappa \sum_{E_j} \int_{\Omega_E} \nabla T \cdot \nabla N_j d\Omega \\ &= \kappa \sum_{E_j} \int_{\Omega_E} \nabla_E T \cdot \nabla_E N_j \left|\det(J_E)\right| d\Omega \\ &= \kappa \sum_{E_j} \sum_{k=1}^{e} \int_{\Omega_E} \nabla_E [N_{gE(k)} T_{gE(k)}] \cdot \nabla_E N_j \left|\det(J_E)\right| d\Omega \\ &= \kappa \sum_{E_j} \sum_{k=1}^{e} \sum_{l=1}^{f} \omega_l [\nabla_E N_{gE(k)}(q_l) \cdot \nabla_E N_j(q_l)] T_{gE(k)} \left|\det(J_E)\right| \end{aligned} \tag{16}$$

where the outermost sum is over those elements E_j that have node j as a vertex, and e is the number of Lagrange linear shape functions per element in this study. The last step in Eq. (16) is the numerical integration using the Newton-Cotes quadrature for the integration in the prior step, so q_l ($l=1,2,..,f$) are quadrature points on the master element and ω_l are the quadrature weights. Additionally, $gE(k)$ is the global node number of node k of element E_j, ∇_E denotes the gradient restricting the master element at point q_l, N is the shape function, and J_E is the Jacobian of the element mapping. In the same way, the convection term in Eq. (15) can be expressed as:

$$\int_{\Omega} (V \cdot \nabla T) N_j d\Omega = \sum_{E_j} \sum_{k=1}^{e} \sum_{l=1}^{f} \{\omega_l [\sum_{k=1}^{e} N_{gE(k)}(q_l) V_{gE(k)}] \cdot \nabla_E N_{gE(k)}(q_l) N_j(q_l)\} T_{gE(k)} \left|\det(J_E)\right| \tag{17}$$

In Eqs. (16) and (17), the non-constant expressions with respect to the node positions are:

$$\nabla_E N_{gE(k)}, \quad \nabla_E N_j, \quad \left|\det(J_E)\right|$$

in each element E. The first two terms are the gradient of the shape function, and the third term is the determinant of the element mapping Jacobian. So the calculation of $\partial S_{5,j}/\partial \xi$ depends on the evaluation of the derivatives of the upper three expressions over the node positions. When node j and boundary nodes at ξ share the same element E, the derivatives of the upper three expressions over the node positions can be computed directly. Readers can refer to Schneider and Jimack (2008) for the calculation details, which are relatively straightforward. Otherwise, $\partial S_{5,j}/\partial \xi$ should be evaluated by the chain rule of differentiation:

$$\frac{\partial S_{5,j}}{\partial \xi} = \frac{\partial S_{5,j}}{\partial \delta}\frac{\partial \delta}{\partial \xi} \tag{18}$$

where node j and the node at coordinates δ share the same element E. Therefore, $\partial S_{5,j}/\partial \delta$ can be directly evaluated, but $\partial \delta/\partial \xi$ cannot be evaluated unless a parametric mesh is used. In the CFD simulation for an indoor environment, the mesh would be too fine to have a mapping between all the nodes, and $\partial \delta/\partial \xi$ cannot be evaluated. However, the contributions of the interior elements away from the air supply diffuser become small very quickly on fine meshes (Schneider, 2006). When node j and ξ do not share the same element E, neglecting $\partial S_{5,j}/\partial \xi$ might be a viable option. This study thus adopted the contributions of the elements that have boundary nodes at ξ as a vertex to evaluate the derivative of the NS equations over the node positions. In summary, $\partial S_5/\partial \xi$ can be computed by:

$$\partial S_5 / \partial \xi = \sum_{j=1}^{n} \partial S_{5,j} / \partial \xi \tag{19}$$

$$\partial S_{5,j} / \partial \xi = 0 \text{ if node } j \text{ and } \xi \text{ do not share the same element } E \tag{20}$$

After $\partial S/\partial \xi$ is determined, the variation of the node positions on the boundary of the air supply diffusers can be computed to determine the new air supply location and size by Eq. (14). Then, the updated ξ is used as input for step 2 in section 2.1 to see if the objective function satisfies the convergence criterion. If not, steps 3 and 4 are repeated to obtain new ξ, which can lead to a smaller O. This approach creates a design cycle that can be repeated until the optimal air supply location and size are achieved.

2.3 Numerical method

In step 2 of section 2.1, the NS equations in this study were the Reynolds-averaged ones with a Re-Normalization Group (RNG) k-ε model (Yakhot and Orszag, 1986), which is widely used for indoor airflow modeling (Zhang et al., 2007; Zhai et al., 2007). To reduce the computational load, this study "froze" the turbulence (Othmer, C. 2008; Dwight and Brezillon, 2006), and the turbulent viscosity in the NS equations was re-used for the adjoint diffusion term. Besides, to simulate the buoyancy effect in indoor airflow, this study adopted Boussinesq approximation (Boussinesq, 1903). In solving the NS/adjoint equations, this study used a semi-implicit method for a pressure-linked equations (SIMPLE) algorithm (Patankar and Spalding, 1972) to couple the velocity/adjoint velocity and pressure/adjoint pressure. All the equations were implemented in OpenFOAM (2007), which is an open source CFD software package.

In the design procedure, the NS/adjoint equations were calculated with M_1/M_2 iterations to ensure the convergence. The design convergence criteria were: (1) $O_{new}<\psi$ in the first design cycle, where ψ is a small positive constant set by the designer and (2) $|O_{new}-O_{old}|<\phi$ after the first design cycle, where O_{old} is the computed objective function in the prior design cycle and ϕ is a small positive constant that was set by the designer. Once the new air supply location and size were obtained in step 4 of section 2.1, this study adopted the Gambit journal files (GAMBIT CFD Preprocessor, 1998) to automatically regenerate the corresponding mesh.

3. Results

This section reports the validation of the CFD-based adjoint method with an attainable design objective and the demonstration of its performance with an ideal design objective. The first case used an example with known air supply location, size, and parameters and airflow fields from the experiment. By using the measured air velocity and temperature in the flow domain as the design

objective, the adjoint method was used to identify the air supply location, size, and parameters. If the air supply location, size, and parameters calculated are the same as the known ones, the adjoint method is thus validated. The second case started with desirable air velocity and temperature distributions in a design domain. The adjoint method was employed to find the corresponding air supply location, size, and parameters. Then, with the air supply location, size, and parameters found as the boundary conditions for forward CFD simulations, the CFD results can be used to verify if the air velocity and temperature distributions in the design domain are the same as the desired ones.

3.1 Validation with an attainable design objective

The validation of the CFD-based adjoint method in the first case used the inverse identification of air supply location, size, and parameters for a two-dimensional, non-isothermal case with experimental data from Blay et al. (1992). In Figure 1(a), the dimensions of the flow domain were H × H = 1.04 m × 1.04 m, the inlet location was $y_{in}/H = 0.991$ (y_{in} is the y coordinate of the middle point of the inlet), the inlet height was h_{in} = 18 mm, and the outlet height was h_{out} = 24 mm. In the experiment, the inlet air velocity was $V_x = 0.57$ m/s, $V_y = 0.0$ m/s, and the inlet air temperature (T_{in}) was 15ºC. The temperature of the walls (T_{wl}) was 15ºC, and that of the floor (T_{fl}) was 35.5ºC to form a thermal plume. The case used here is representative of airflows in enclosed environments as it includes major flow characteristics in an indoor environment, such as jets and thermal plumes. Furthermore, it was not desirable to use very complex cases for this investigation since those cases may have uncertainties. Instead, this simple two-dimensional case, but still with complex flow features, was more desirable for validation.

The experiment by Blay et al. (1992) measured the air velocity and temperature on red dash lines, as shown in Figure 1(a). Our inverse simulation thus set the measured air velocity and temperature as a design objective for simplification. This is because any complex design objective in an enclosed environment such as PMV or the age of the air is based on flow and/or temperature fields. Then the objective function for this case can be constructed as:

$$O(\xi) = \alpha \int_{\theta} (V - V_0)^2 \, d\theta + \beta \int_{\theta} (T - T_0)^2 \, d\theta \tag{21}$$

where α and β were chosen to adjust the relative importance of the two integrals and θ denotes the design domain represented by the red dash lines in Figure 1(a). This design objective was clearly attainable because it measured data from the experiment with the corresponding boundary conditions used. The boundary conditions were velocity V_x =0.57 m/s and V_y = 0, temperature 15ºC, location $y_{in}/H = 0.991$, and size h_{in} = 0.018 m of the air supply and wall surface temperatures. Thus, the inverse simulation, if successful, must be able to find the boundary conditions. Figure 1(b) shows the resolution of the mesh when the inlet was located at $y_{in}/H = 0.991$. The mesh resolution at the inlet, outlet, and near wall region was finer because of the high gradient of velocity and temperature there. This principle was applied to regenerate the mesh when the air supply location and size changed in the calculation.

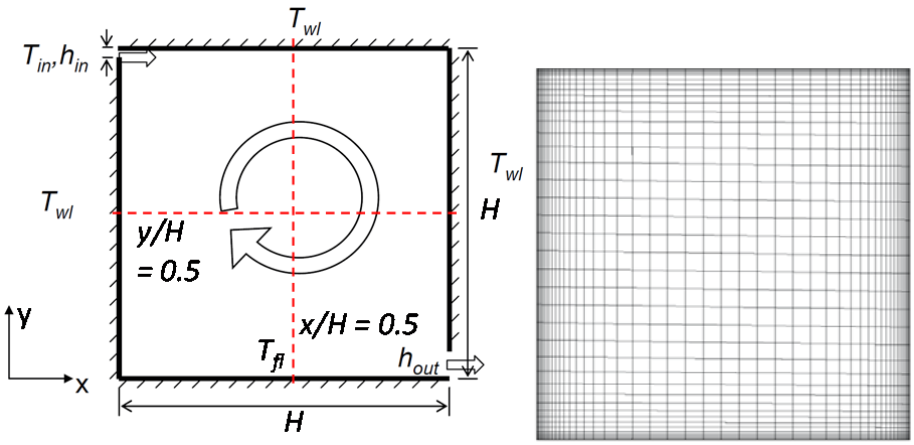

(a) *(b)*

Figure 1. Sketch (a) and mesh (b) of the two-dimensional, non-isothermal case

To inversely identify the air supply location, size, and parameters, a number of design variables were added one by one to test the robustness of the method:

- Scenario 1-1: Inverse identification of the air supply location.
- Scenario 1-2: Inverse identification of the air supply location and supply parameters.
- Scenario 1-3: Inverse identification of the air supply location, size, and supply parameters.

Scenario 1-1 used the air supply location as a design variable. The air supply size and parameters were fixed at h_{in} = 0.018 m, V_x = 0.57 m/s, V_y = 0 m/s, and T_{in} = 15ºC, respectively. Therefore, the optimal air supply location should be y_{in}/H = 0.991. Scenario 1-2 assumed the air supply parameters to be unknown. However, the airflow rate was constrained by:

$$(V_{in} \cdot \vec{n}) h_{in} = Q \tag{22}$$

where Q = 0.01026 m^2/s in this study. Scenario 1-3 further assumed that the inlet size was a design variable. Table 1 summarizes the detailed thermo-fluid conditions for the three scenarios.

Table 1. Summary of the studied scenarios

Scenario	Design variables	Objective function	Fixed boundary conditions	Initial conditions	ψ	ϕ	M_1	M_2
1-1	y_{in}	Eq. (21) with α = 1, β = 1	$V_{x,in}$ = 0.57 m/s, $V_{y,in}$ = 0 m/s, T_{in} = 15ºC, h_{in} = 0.018 m, T_{wl} = 15 ºC, T_{fl} = 35.5ºC	y_{in}/H = 0.5	10^{-2}	10^{-2}	7000	7000
1-2	y_{in}, $V_{y,in}$, T_{in}	Eq. (21) with α = 1, β = 1	Q = 0.01026 m^2/s, h_{in} = 0.018 m, T_{wl} = 15 ºC, T_{fl} = 35.5ºC	y_{in}/H = 0.5, $V_{y,in}$ = 0.2 m/s, T_{in}=10 ºC				

1-3	y_{in}, $V_{x,\,in}$, $V_{y,\,in}$, T_{in}, h_{in}	Eq. (21) with α = 1, β = 1	Q = 0.01026 m^2/s, T_{wl} = 15 ºC, T_{fl} = 35.5ºC	y_{in}/H = 0.5, h_{in} = 0.0342 m, $V_{x,\,in}$ = 0.3 m/s,, $V_{y,\,in}$ = 0.2 m/s, T_{in}=10 ºC				

Figure 2(a) shows that all the inverse calculations led the variation of objective function $|O_{new}-O_{old}|$ to be smaller than 10^{-2} so the convergence criterion was achieved. The design cycle is the number of updating design variables. Therefore, this method could inversely identify the local optimal design variables. The convergence speed of the three scenarios was similar. The increase in design variables would not increase the computational effort, which is a strong feature of the adjoint method. Although all the calculations had similar values to the design objective, the optimal air supply location, size, and parameters obtained differed significantly, as shown in Figure 2(b). This was due to the different combinations of air supply location, size, and parameters, which could lead to similar air distributions at the design domain and indicated the existence of multiple local optima.

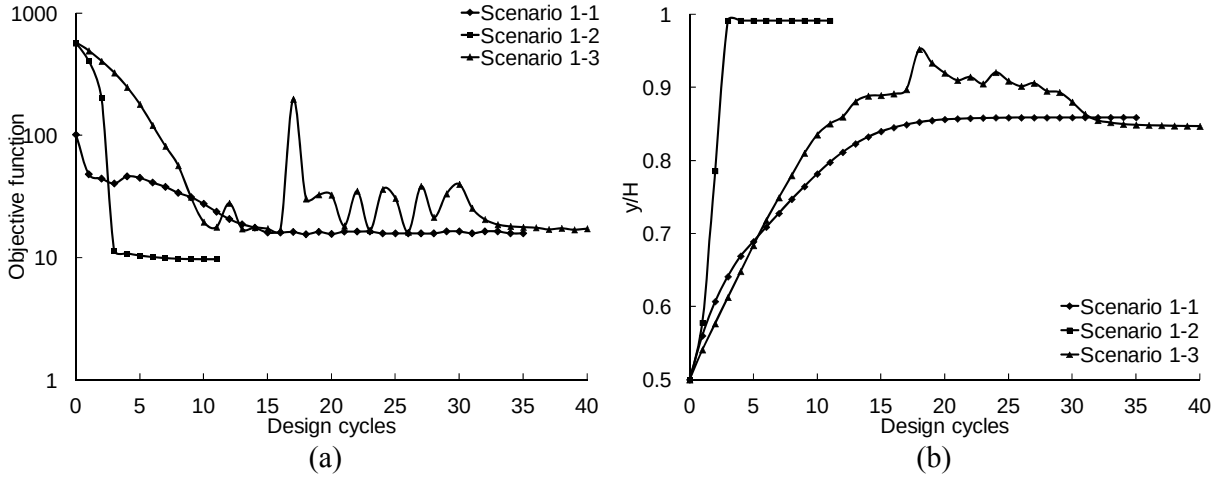

Figure 2. (a) Objective function and (b) inlet location determined versus design cycles (number of updating the design variables)

The objective function for Scenario 1-3 had a sudden jump at design cycle 16. The reason was that the flow feature at design cycle 17 had a sudden change, as shown in Figure 3(c). As depicted in Figure 4, the temperature profiles changed a lot as well. The objective function for Scenario 1-3 still had fluctuations after design cycle 20. The reason was that the inlet was close to the upper wall and its location fluctuated. The fluctuation in the air supply location (Figure 3(b)) did not much change the flow field, but did influence the heat transfer between the jet and the upper wall. In Figure 5, the velocity profiles of design cycles 20 and 21 did not change much, but the temperature profiles differed a lot. Figure 3(d) shows the optimal flow field at design cycle 40 for Scenario 1-3. The flow field differed significantly from that for the initial condition, as shown in Figure 3(a).

When setting the air supply size as a design variable in Scenario 1-3, the air supply velocity in the x direction was also a design variable due to the requirement of a constrained air flow rate. The computed results by this CFD-based adjoint method would provide the variations of the air supply size h_{in} and air supply velocity in the x direction $V_{x,\,in}$ at the same time. When both of them change, it is hard or impossible to maintain a constant air flow rate. Therefore, this study varied $V_{x,\,in}$ to determine the air supply size h_{in} by using Eq. (22). The results in Figure 4 show that this treatment works well for the inverse identification of air supply size in an enclosed environment.

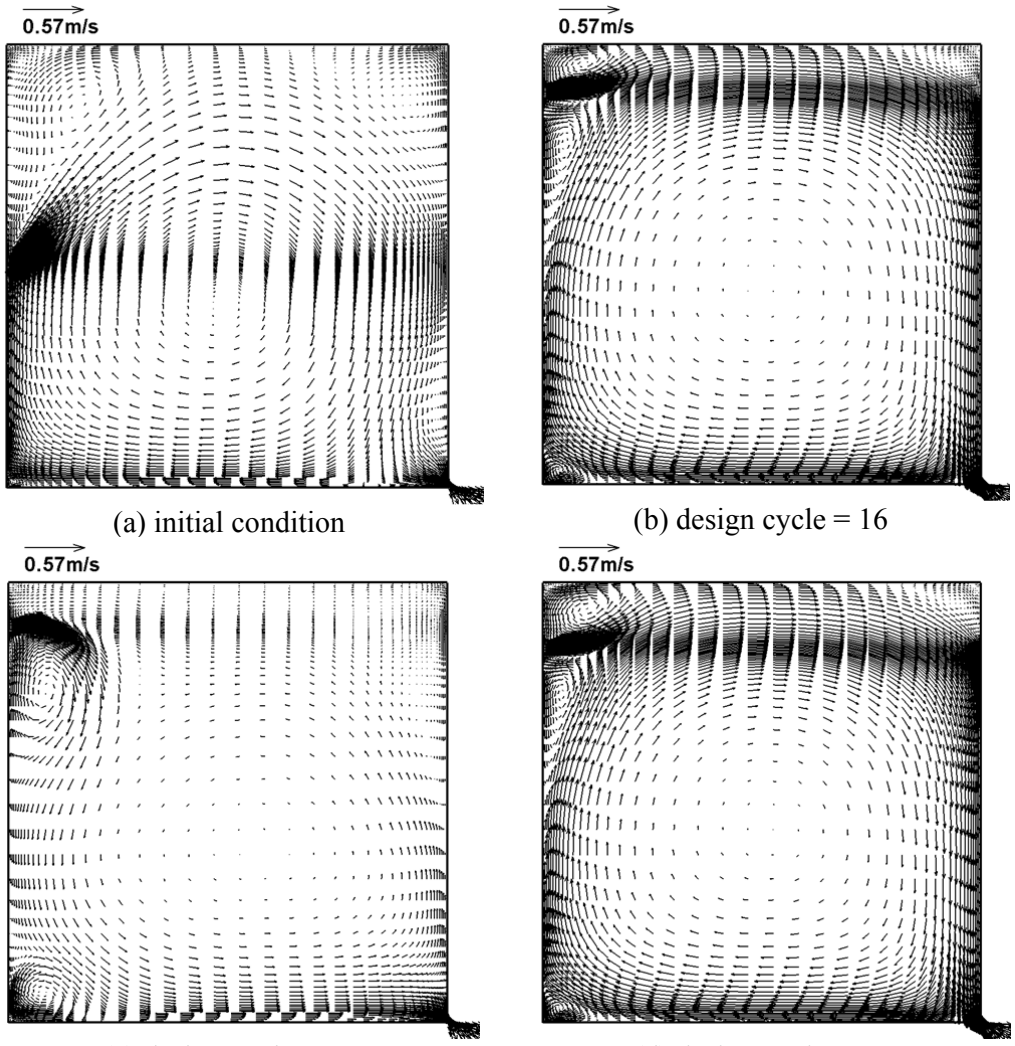

(a) initial condition (b) design cycle = 16

(c) design cycle = 17 (d) design cycle = 40

Figure 3. Computed flow fields at (a) initial condition, (b) design cycle (number of updating the design variables) 16, (c) design cycle 17, and (d) design cycle 40 for Scenario 1-3.

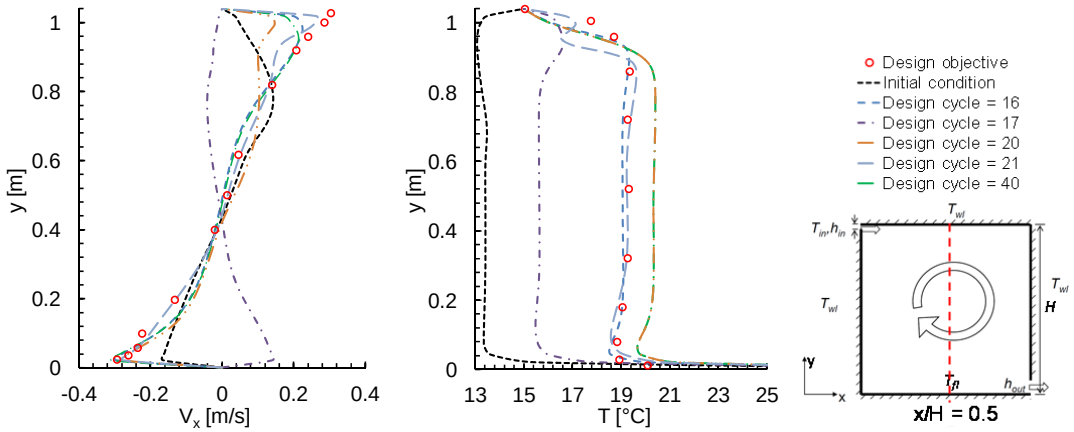

Figure 4. Comparison of the velocity and temperature profiles determined by the adjoint method and the design objective at x/H = 0.5 for Scenario 1-3.

The air supply location, size, and parameters obtained by the CFD-based adjoint method were then used as inputs for forwarded CFD simulations to calculate the air distribution in the cavity. Figures 5 shows the velocity and temperature profiles at x/H=0.5 calculated by the forwarded CFD simulations with the air supply location, size, and parameters. Comparing the profiles with the design objective (Blay et al., 1992) at x/H = 0.5, only the velocity profiles near the top wall displayed a minor difference from the design objective. This indicates that multiple solutions of air supply location, size, and parameters can be obtained by the adjoint method and all the solutions can lead to similar design objectives.

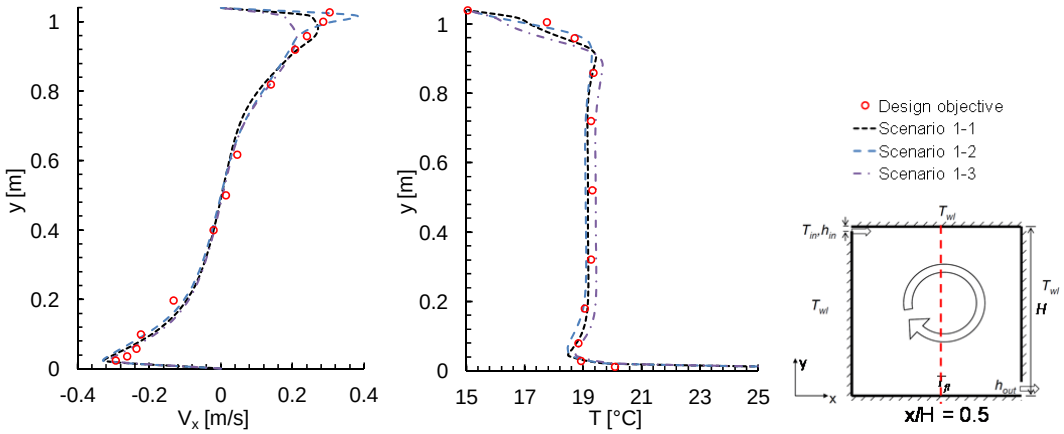

Figure 5. Comparison of the optimal velocity and temperature profiles determined by the adjoint method with the design objective at x/H = 0.5.

3.2 Demonstration of the adjoint method with an ideal design objective

The second case was to demonstrate how the CFD-based adjoint method can be used to obtain air supply location, size, and parameters with an ideal design objective in a design domain. Based on the two-dimensional, non-isothermal case used in Section 3.1, this investigation set desired air velocity of $V_{0,\,x}$ = 0.1 m/s and $V_{0,\,y}$ = 0 m/s and desired air temperature of T_0 = 22 °C in the design domain θ as (the red dash line from y = 0.05 m to 0.5 m in Figure 6). The design domain is analogous to the height from the ankle to the head of an occupant in the middle of the occupied zone in a room. Then Eq. (21) was again used as the objective function.

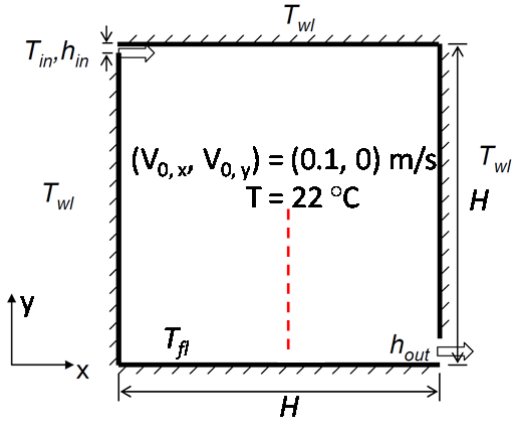

Figure 6. An ideal design objective for the two-dimensional, non-isothermal case by setting air velocity and temperature profiles on the red dash line.

This study conducted the optimization with three scenarios. The first two scenarios were constrained by airflow rate in Eq. (22) and were with two arbitrarily initial air supply location and air supply parameters. For example, Scenario 2-1 had the initial air supply location in the middle of the left wall ($y_{in}/H = 0.5$) while Scenario 2-2 had the air supply location at the lower end of the left wall ($y_{in}/H = 0.025$). Scenario 2-3 did not have the constraint on the airflow rate arbitrarily set its initial conditions. Table 2 summarizes the detailed information for the three scenarios.

Table 2. Summary of the studied scenarios

Scenario	Design variables	Objective function	Fixed values	Initial air supply conditions	ψ	ϕ	M_1	M_2
2-1	y_{in}, $V_{x,in}$, $V_{y,in}$, T_{in}, h_{in}	Eq. (21) with $\alpha = 100$, $\beta = 1$	$Q = 0.01026$ m^2/s, $T_{wl} = 15$ ºC, $T_{fl} = 35.5$ºC	$y_{in}/H = 0.5$, $h_{in} = 0.0513$ m, $V_{x,in} = 0.2$ m/s,, $V_{y,in} = -0.2$ m/s, $T_{in} = 10$ ºC	10^{-1}	10^{-1}	7000	7000
2-2				$y_{in}/H = 0.025$, $h_{in} = 0.0513$ m, $V_{x,in} = 0.2$ m/s,, $V_{y,in} = 0$ m/s, $T_{in} = 10$ ºC				
2-3			$T_{wl} = 15$ ºC, $T_{fl} = 35.5$ºC	$y_{in}/H = 0.049$, $h_{in} = 0.1026$ m, $V_{x,in} = 0.1$ m/s,, $V_{y,in} = 0$ m/s, $T_{in} = 20$ ºC				

Figure 7(a) shows that the variation of the objective function $|O_{new}-O_{old}|$ in all three scenarios can be smaller than 10^{-1} with more than 50 design cycles. This means the convergence was achieved although the optimal air supply locations were different, as shown in Figure 7(b). Therefore, this method could inversely identify local optimal air supply location, size and parameters. Scenario 2-1 had a sudden jump at the 19th design cycle for the objective function due to a rapid change in the flow pattern, as depicted in Figure 8. The flow at the lower part of the cavity at design cycle 18 was clockwise and became counter-clockwise at design cycle 19. The optimization process can change the flow fields dramatically. Figure 9 further shows that the change in the flow features made the temperature profiles differ a lot. We can also see that the optimal velocity and temperature profiles at design cycle 46 for Scenario 2-1 differed significantly from the initial condition.

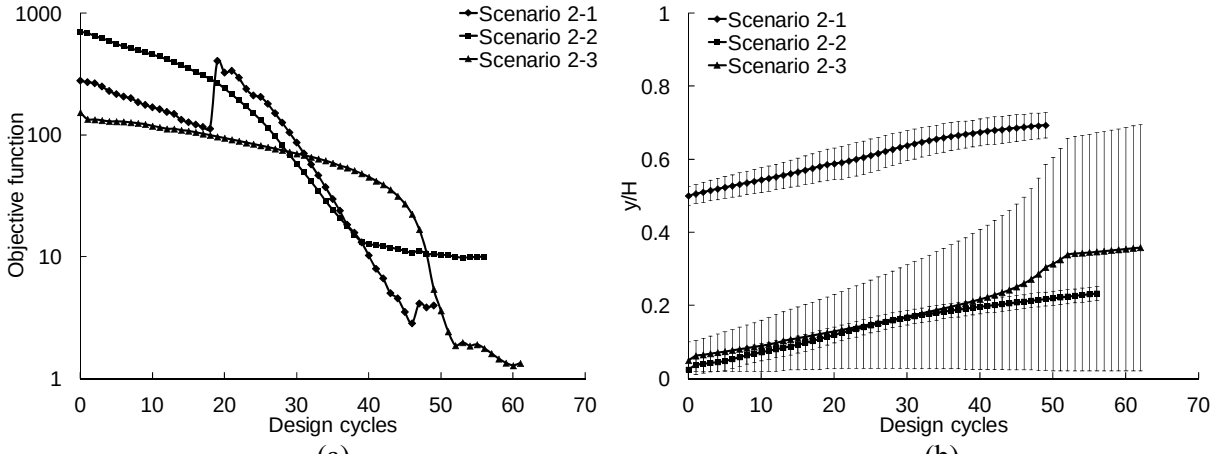

Figure 7. (a) Objective function and (b) inlet location (solid lines) and size (vertical bars) determined versus design cycle (number of updating the design variables).

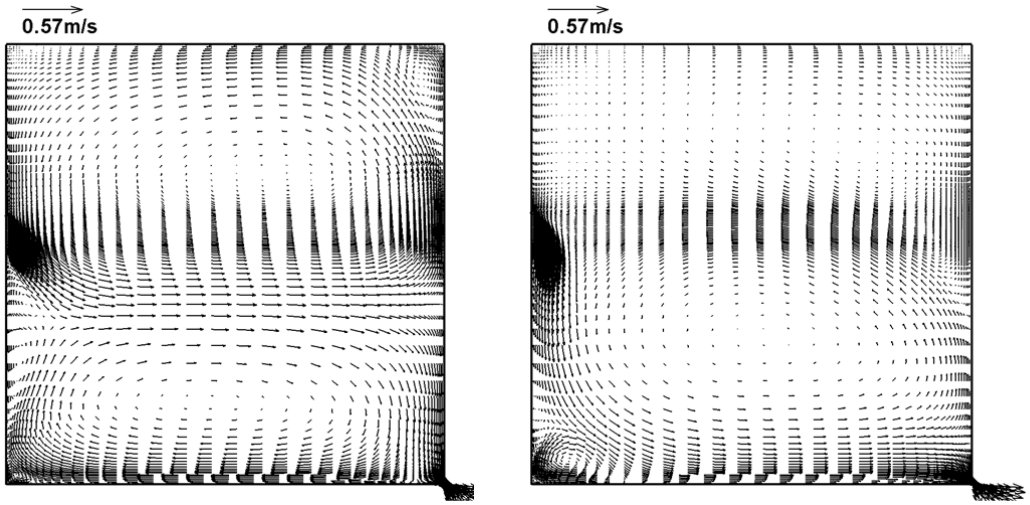

(a) Design cycle = 18 (b) Design cycle = 19

Figure 8. Computed flow fields at (a) design cycle (number of updating the design variables) 18 and (b) design cycle 19 for Scenario 2-1.

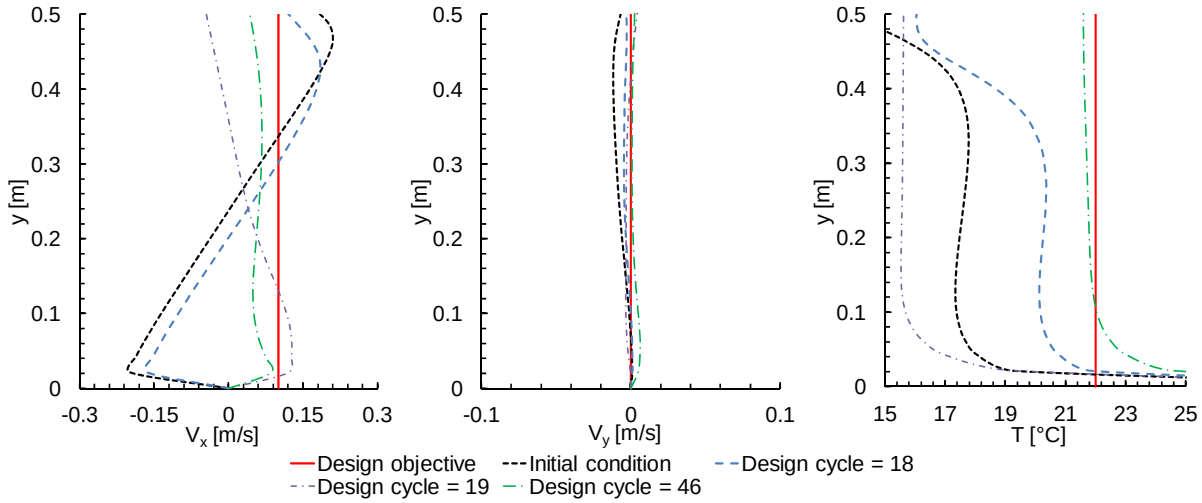

Figure 9. Comparison of the velocity and temperature profiles determined by CFD with air supply location, size, and parameters obtained by the adjoint method and the design objective on the design domain for Scenario 2-1.

The vertical bars in Figure 7(b) show the inlet size variations versus the design cycles. At the optimal condition, the inlet size of the three scenarios was 0.0725 m, 0.0384 m, and 0.7018 m, respectively. The airflow rate at the optimal condition for Scenario 2-3 was 0.07199 m^2/s, which was about seven times higher than the constrained airflow rate for Scenarios 2-1 and 2-2. Figure 10 shows the velocity and temperature profiles calculated by the forwarded CFD simulation with the air supply location, size, and parameters obtained by the adjoint method as inputs. With the constrained airflow rate, the velocity and temperature profiles obtained deviated significantly from the desired design objective. Only the air velocity and temperature profiles for Scenarios 2-3 were similar to those set in the objective function. This means that the desirable design objective can only be obtained with sufficient freedom to choose the corresponding boundary conditions.

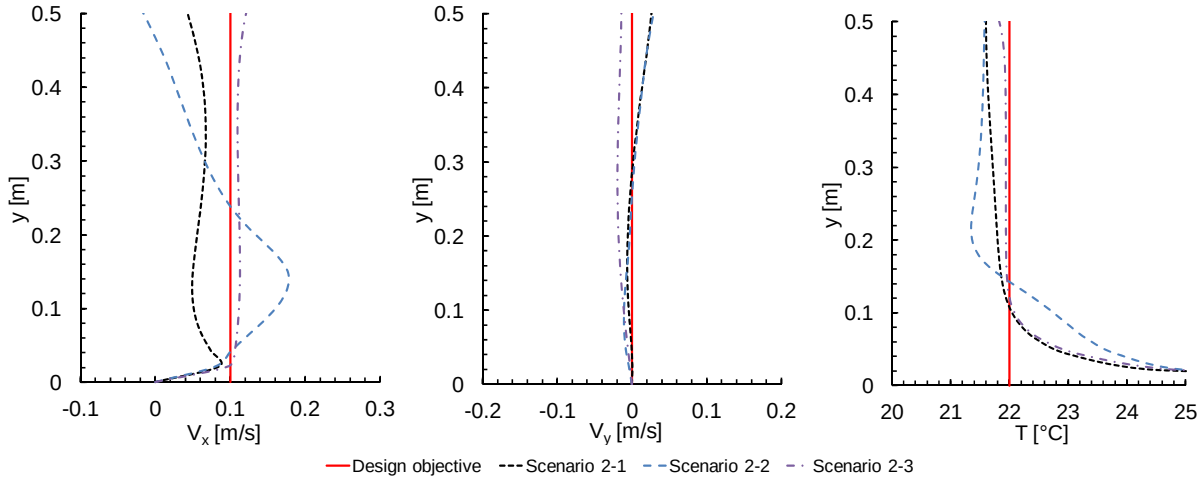

Figure 10. Comparison of the optimal velocity and temperature profiles determined by the adjoint method under different constraint conditions with the design objective.

4. Discussions

The calculations in sections 3.1 and 3.2 both converged, but led to different values for the objective functions. In Section 3.1, the objective function was expected to be zero if the experimental data had no errors and the predicted air distributions by CFD simulation were the same as the experimental data. However, the experimental data inevitably had errors as the measuring instruments had uncertainties and the turbulence models used in the CFD simulation had approximations. The predicted air velocity and temperature profiles by CFD simulation in the design procedures thus had differences from the design objective. These explain the relatively large final objective functions in section 3.1. In section 3.2, the final objective functions of scenarios 2-1 and 2-2 differed because of the existence of multiple solutions. Further, the final objective function of scenario 2-3 was much smaller than that in section 3.1. The possible reasons were a smaller design domain and more freedom to choose the corresponding boundary conditions in scenario 2-3.

The CFD-based adjoint method for the two-dimensional cases can yield multiple optimal solutions even with a single design variable. It requires multiple trials to obtain the global optimal solutions, which would be time-consuming. To improve the computational efficiency, one may first take advantage of the CFD-based GA method to determine the initial air supply locations and parameters, which may lead to multiple solutions. Then, the optimization with the CFD-based adjoint method can be conducted with these pre-determined initial air supply locations and parameters to check if these initial conditions would lead to a unique solution. Theoretically, the combined CFD-based GA and adjoint method can be faster than the pure CFD-based GA and can find the global optima that makes up for the shortcomings of the pure CFD-based adjoint method. For example, Xue and Zhai (2007) recently tried to accelerate the GA method by integrating with the adjoint method. This new integrated method has a great advantage when the number of variables for optimization is large. In addition, our future study will try to solve the NS/adjoint equations by fast fluid dynamics (Zuo and Chen, 2009), which can further decrease the computational effort.

The major simplifications in this study were on design variables and the adjoint of turbulence models. For example, we assumed the inlet air velocity to be uniform. The simplifications on the design variables make it easier to show the strength of the method, although the adjoint method can handle more complex cases. This study also simplified the turbulence models used in the adjoint equations by "frozing" the turbulence level in order to reduce the computing time. According to Dwight and Brezillon (2006), the accuracy of approximating the turbulence was case dependent. Fortunately, the simplification seemed acceptable in our case.

5. Conclusions

This study presented a CFD-based adjoint method for inverse identification of air supply location, size, and parameters. The method used local contributions of the derivative of the NS equations over the node positions by FEM. This method was tested by applying it to a two-dimensional, ventilated cavity. The study led to the following conclusions:

- By using the measured air velocity and temperature in several locations in a ventilated cavity, the CFD-based adjoint method can identify the air supply location, size, and parameters that can lead to the same air velocity and temperature in those locations. However, the results show that different air supply location, size, and parameters could result in the same air velocity and temperature in those locations. This implies that multiple solutions exist and can be identified by the method.
- By using different air supply location, size, and parameters as design variables, the adjoint method could simultaneously identify the locally optimal design variables. The computing costs did not vary with the number of design variables.
- This study has successfully demonstrated that it is possible to set desirable design objectives in the flow domain and to obtain the corresponding air supply location, size, and parameters needed for achieving the design objective. The initial boundary conditions can be arbitrarily set. With different constraints used, the air supply location, size, and parameters found can be very different.

Acknowledgments

The research presented in this paper was supported financially by the National Basic Research Program of China (The 973 Program) through Grant No. 2012CB720100.

Nomenclature

Symbol definition

d	variation
D	rate of strain tensor
e	number of Lagrange linear shape functions per element
E	element
$\vec{g}$	gravity vector
gE(k)	global node number of node k of element E
h	air supply size
J	Jacobian of element mapping
L	augmented objective function
M	iteration number
n	number of internal nodes
N	shape function
$\vec{n}$	unit vector in the normal direction
O	objective function
p	pressure
q	quadrature point
Q	airflow rate
S	Navier-stokes equations, vector form
T	air temperature
V	air velocity, vector

x, y	index of coordinates

Subscripts

0	design objective
1, 2, 3, 4, 5	component of a vector
a	adjoint parameter
fl	value at the floor
i	component of a vector
initial	initialized value
in	value at the air supply inlet
j	node number
l	quadrature point number
old	value at prior design cycle
new	value updated at current design cycle
op	operating value
outlet	value at the outlet
wl	value at the wall
x, y	component in the x and y direction, respectively

Greek symbols

α, β	weighting factor, positive constant
γ	thermal expansion coefficient
δ	node coordinates
θ	design domain
κ	effective conductivity
λ	step size, positive constant
ν	effective viscosity
ξ	design variable, vector
ψ	positive constant
ω	quadrature weight
ϕ	positive constant
Ω	computation domain

References

ASHRAE. 2010. ANSI/ASHRAE Standard 62.1-2010, Ventilation for acceptable indoor air quality. American Society of Heating, Refrigerating, and Air-Conditioning Engineers, Atlanta, GA.

Blay, D., Mergui, S., Niculae, C. 1992. Confined turbulent mixed convection in the presence of a horizontal buoyant wall jet, Fundamentals of Mixed Convection. ASME HTD, 213, 65-72.

Boussinesq, J. 1903. Theorie Analytique de la Chaleur. Gauthier-Villars.

Bryson, A.E., Ho, Y.C. 1975. Applied Optimal Control. Hemisphere, Washington, DC.

Dwight, R.P., Brezillon, J. 2006. Effect of various approximations of the discrete adjoint on gradient-based optimization. Proceedings of the 44th AIAA Aerospace Sciences Meeting and Exhibit, Reno, NV.

GAMBIT CFD Preprocessor. 1998. User's Guide. Lebanon, NH: Fluent Inc.

Giles, M.B., Pierce, N.A. 2000. An introduction to the adjoint approach to design. Flow, turbulence and combustion, 65(3-4), 393-415.

Gill, P.E., Murray, W., Wright, M.H. 1981. Practical optimization. Academic Press.

Griwank, A. 2000. Evaluating Derivatives, Principles and Techniques of Algorithmic Differentiation. SIAM.

Gunzburger, M.D. 2003. Perspectives in flow control and optimization. SIAM.
Haasdonk, B., Ohlberger, M. 2011. Efficient reduced models and a posteriori error estimation for parametrized dynamical systems by offline/online decomposition. Mathematical and Computer Modelling of Dynamical Systems, 17(2), 145-161.
Hedge, A., Erickson, W. A., Rubin, G. 1996. Predicting sick building syndrome at the individual and aggregate levels. Environment International, 22(1), 3-19.
Holland, J. 1975. Adaptation in Natural and Artificial Systems, Ann Arbor, University.
International Facility Management Association. 2003. Too cold and too hot rank at top of workplace complaints.
Jameson, A. 1995. Optimum aerodynamic design using CFD and control theory. AIAA paper, 1729, 124-131.
Jameson, A., Martinelli, L., Pierce, N.A. 1998. Optimum aerodynamic design using the Navier–Stokes equations. Theoretical and Computational Fluid Dynamics, 10(1-4), 213-237.
Jimack, P.K. 1997. An optimal finite element mesh for elastostatic structural analysis problems. Computers and Structures, 64(1), 197-208.
Kämpf, J.H., Wetter, M., Robinson, D. 2010. A comparison of global optimization algorithms with standard benchmark functions and real-world applications using EnergyPlus. Journal of Building Performance Simulation, 3(2), 103-120.
Li, K., Su, H., Chu, J., Xu, C. 2012. A fast-POD model for simulation and control of indoor thermal environment of buildings. Building and Environment, 60,150-157.
Li, K., Xue, W., Xu, C., Su, H. 2013. Optimization of ventilation system operation in office environment using POD model reduction and genetic algorithm. Energy and Buildings, 67, 34-43.
Liu, W. and Chen, Q. 2014. Optimal air distribution design in enclosed spaces using an adjoint method, submitted to Inverse Problems in Science & Engineering.
Mendell, M.J. 1993. Non-specific symptoms in office workers: a review and summary of the epidemiologic literature. Indoor Air, 3(4), 227-236.
Menzies, R.D., Pasztor, J., Leduc, J., Nunes, F. 1994. The 'sick building'–a misleading term that should be abandoned. In Indoor Air Quality, 37-48.
Nguyen, A.T., Reiter, S. 2014. Passive designs and strategies for low-cost housing using simulation-based optimization and different thermal comfort criteria. Journal of Building Performance Simulation, 7(1), 68-81.
OpenFOAM. 2007. The Open Source CFD Toolbox. http://www.opencfd.co.uk/openfoam.html.
Othmer, C. 2008. A continuous adjoint formulation for the computation of topological and surface sensitivities of ducted flows. International Journal for Numerical Methods in Fluids, 58, 861-877.
Patankar, S.V., Spalding, D.B. 1972. A calculation procedure for heat, mass and momentum transfer in three-dimensional parabolic flows. International Journal of Heat and Mass Transfer, 15(10), 1787-1806.
Rozza, G., Huynh, D., Patera, A. 2007. Reduced basis approximation and a posteriori error estimation for affinely parametrized elliptic coercive partial differential equations. Archives of Computational Methods in Engineering, 15(3), 1-47.
Schneider, R. 2006. Applications of the discrete adjoint method in computational fluid dynamics. Doctoral dissertation, The University of Leeds.
Schneider, R., JIMACK, P. K. 2008. On the evaluation of finite element sensitivities to nodal coordinates. Electronic Transactions on Numerical Analysis, 32, 134-144.
Sokolowski, J., Zolesio, J.P. 1992. Introduction to shape optimization. Springer Berlin Heidelberg.
U.S. Department of Energy. 2011. Building energy data book. http://buildingsdatabook.eren.doe.gov/ChapterIntro1.aspx
Wikipedia, Http://en.wikipedia.org/wiki/Automatic_differentiation.
Wright, J.A., Brownlee, A., Mourshed, M.M., Wang, M. 2014. Multi-objective optimization of cellular fenestration by an evolutionary algorithm. Journal of Building Performance Simulation, 7(1), 33-51.

Xue, Y., Zhai, Z., Chen, Q. 2013. Inverse prediction and optimization of flow control conditions for confined spaces using a CFD-based genetic algorithm. Building and Environment, 64, 77-84.
Xue, Y., Zhai, Z. 2014. Comparison and integration of generic algorithm and adjoint algorithm for optimizing indoor environments. Proceedings of the 13th International Conference on Indoor Air Quality and Climate (Indoor Air 2014).
Yakhot, V., Orszag, S.A. 1986. Renormalization group analysis of turbulence. Journal of Scientific Computing, 1(1), 3-51.
Zhai, Z., Zhang, Z., Zhang, W., Chen, Q. 2007. Evaluation of various turbulence models in predicting airflow and turbulence in enclosed environments by CFD: part-1: summary of prevalent turbulence models. HVAC&R Research, 13(6), 853-870.
Zhang, Z., Zhang, W., Zhai, Z., Chen, Q. 2007. Evaluation of various turbulence models in predicting airflow and turbulence in enclosed environments by CFD: part-2: Comparison with experimental data from literature. HVAC&R Research, 13(6), 871-886.
Zhou, L., Haghighat, F. 2009. Optimization of ventilation system design and operation in office environment, Part I: Methodology. Building and Environment, 44(4), 651-656.
Zhou, L., Haghighat, F. 2009. Optimization of ventilation systems in office environment, Part II: Results and discussions. Building and Environment, 44(4), 657-665.
Zuo, W., Chen, Q. 2009. Real time or faster-than-real-time simulation of airflow in buildings. Indoor Air, 19(1), 33-44.